1521-0111/92/1/1–11$25.00
MOLECULAR PHARMACOLOGY

https://doi.org/10.1124/mol.117.108514
Mol Pharmacol 92:1–11, July 2017

MINI SPECIAL SECTION—STRUCTURAL BASIS OF RECEPTOR-LIGAND INTERACTIONS

Structure and Dynamics of the Liver Receptor Homolog 1–PGC1α Complex

Suzanne G. Mays, C. Denise Okafor, Micheal L. Tuntland, Richard J. Whitby, Venkatasubramanian Dharmarajan, Józef Stec, Patrick R. Griffin, and Eric A. Ortlund

Department of Biochemistry, Emory University School of Medicine, Atlanta, Georgia (S.G.M., C.D.O., M.L.T., E.A.O.); School of Chemistry, University of Southampton, Southampton, United Kingdom (R.J.W., J.S.); and Department of Molecular Medicine, Scripps Research Institute, Jupiter, Florida (V.D., P.R.G.).

Received February 1, 2017; accepted March 29, 2017

ABSTRACT

Peroxisome proliferator-activated gamma coactivator 1-α (PGC1α) regulates energy metabolism by directly interacting with transcription factors to modulate gene expression. Among the PGC1α binding partners is liver receptor homolog 1 (LRH-1; NR5A2), an orphan nuclear hormone receptor that controls lipid and glucose homeostasis. Although PGC1α is known to bind and activate LRH-1, mechanisms through which PGC1α changes LRH-1 conformation to drive transcription are unknown. Here, we used biochemical and structural methods to interrogate the LRH-1–PGC1α complex. Purified, full-length LRH-1, as well as isolated ligand binding domain, bound to PGC1α with higher affinity than to the coactivator, nuclear receptor coactivator-2 (Tif2), in coregulator peptide recruitment assays. We present the first crystal structure of the LRH-1–PGC1α complex, which depicts several hydrophobic contacts and a strong charge clamp at the interface between these partners. In molecular dynamics simulations, PGC1α induced correlated atomic motion throughout the entire LRH-1 activation function surface, which was dependent on charge-clamp formation. In contrast, Tif2 induced weaker signaling at the activation function surface than PGC1α but promoted allosteric signaling from the helix 6/β-sheet region of LRH-1 to the activation function surface. These studies are the first to probe mechanisms underlying the LRH-1–PGC1α interaction and may illuminate strategies for selective therapeutic targeting of PGC1α-dependent LRH-1 signaling pathways.

Introduction

Liver receptor homolog 1 (LRH-1) is an orphan nuclear receptor (NR) that acts as an important regulator of lipid and glucose metabolism. It is highly expressed in liver, where it controls bile acid biosynthesis (Lu et al., 2000), de novo lipogenesis (Lee et al., 2011), and reverse cholesterol transport (Schoonjans et al., 2002; Stein et al., 2014). Notably, activation of LRH-1 in obese mice improves glucose tolerance and insulin resistance (Lee et al., 2011), as well as reduces atherosclerosis formation (Stein et al., 2014). LRH-1 also plays key roles in the resolution of hepatic endoplasmic reticulum stress (Mamrosh et al., 2014) and maintenance of the one-carbon pool (Wagner et al., 2016), which are both critical for metabolic homeostasis and cell survival. Glucose transport, metabolism, and capture are regulated by LRH-1 via control of proteins such as the GLUT4 transporter in skeletal muscle and glucokinase in the liver (Oosterveer et al., 2012; Bolado-Carrancio et al., 2014). On the other hand, aberrant activation of LRH-1 drives tumorigenesis and tumor-cell proliferation in several cancer types (Chand et al., 2010; Thiruchelvam et al., 2011; Bianco et al., 2014; Lin et al., 2014; Bayrer et al., 2015; Nadolny and Dong, 2015; Xu et al., 2016). Because of this vital transcriptional program, LRH-1 is garnering attention as a new therapeutic target for treatment of diseases such as nonalcoholic fatty liver disease, diabetes, and cancer.

As with other NRs, transcriptional activity of LRH-1 relies upon associations with coregulators, a diverse family of proteins that act as chromatin-remodeling factors (or which recruit such factors) to control promoter accessibility. Coregulator interactions typically occur at the NR activation function surface (AFS),

This work was supported in part by the National Institutes of Health [Grants T32-GM008602, F31-DK111171, R01-DK095750, K12-GM000680, 1S10RR027270, and R01-DK105825] and an Emory Catalyst Grant. R.J.W. and J.S. thank GlaxoSmithKline for generous funding.
https://doi.org/10.1124/mol.117.108514.

ABBREVIATIONS: AF-B, alternative activation function surface; AF-H, activation function helix; AFS, activation function surface; DLPC, dilauroylphosphatidylcholine; FAM, fluorescein; FL, full length; HDX, hydrogen-deuterium exchange; HDX-MS, HDS mass spectrometry; LBD, ligand binding domain; LRH-1, liver receptor homolog 1; MD, molecular dynamics; MDS, molecular dynamics simulations; NR, nuclear receptor; PDB, Protein Data Bank; PGC1α, peroxisome proliferator-activated gamma coactivator 1-α; RR-RJW100, (1S,3aS)-5-hexyl-4-phenyl-3a-(1-phenylvinyl)-1,2,3,3a,6,6a-hexahydropentalen-1-ol; SHP, small heterodimer partner; SMRT, silencing mediator of retinoic acid and thyroid hormone receptor; TEV, tobacco etch virus; TIF2, nuclear receptor coactivator-2.

located in the ligand binding domain (LBD). When the AFS is in the active conformation (e.g., upon binding of an activating ligand), coactivators bind to a canonical cleft within this surface via a helical LXXLL motif to drive NR activity (where L is leucine and X is any amino acid). Corepressors inhibit NR activity by binding to an alternative conformation of the AFS using an extended leucine-rich motif. In addition, atypical corepressors [such as small heterodimer partner (SHP)] use an LXXLL-containing helix to compete with coactivators for binding the active AFS, resulting in suppression of NR activity. Interestingly, a phospholipid LRH-1 agonist with antidiabetic effects (Lee et al., 2011) completely ablates SHP binding while preserving the ability to bind coactivators (Musille et al., 2012). This effect is mediated through ligand-driven allosteric communication between the AFS and a distal portion of the LBD, which is now considered an "alternate" AFS (hereafter, AF-B) (Musille et al., 2012, 2016).

Among the LRH-1 coregulators is peroxisome proliferator-activated gamma coactivator 1-α (PGC1α), which plays a critical role in energy homeostasis by interacting with a variety of NRs and other transcription factors (Lin et al., 2005; Finck and Kelly, 2006). PGC1α is expressed in tissues with high demand for energy, such as heart, skeletal muscle, and brown adipose tissue, as well as in the liver. It is expressed at low basal levels but is highly inducible upon certain stimuli, such as cold exposure, during exercise, and signaling from adenosine monophosphate-activated protein kinase, Sirtuin, and cAMP (Finck and Kelly, 2006). Downstream effects of PGC1α activation include stimulation of mitochondrial biogenesis and increased rates of cellular respiration (Finck and Kelly, 2006). In the liver, PGC1α plays a major role in oxidative metabolism, including the control of bile acid production (Lin et al., 2005). PGC1α has several overlapping biologic roles with LRH-1, including in disease states such as obesity, diabetes, and cancer (Lin et al., 2005), and the ability of PGC1α to act as an LRH-1 coactivator has been documented in several studies. The two proteins directly interact via the PGC1α NR box 2 and the LRH-1 AFS (Shin and Osborne, 2008). Overexpression of PGC1α enhances LRH-1 activity at the aromatase and SHP promoters in luciferase reporter assays (Safi et al., 2005), and PGC1α drives expression of CYP7A1 in hepatocytes (Shin and Osborne, 2008). On the other hand, the similar PGC1β isoform cannot activate LRH-1 (Shin and Osborne, 2008). Interestingly, PGC1α appears to be better able to discriminate between LRH-1 ligand-bound states than the nuclear receptor coactivator-2 (Tif2) coactivator, since PGC1α is unable to bind apo-LRH-1 in vitro, whereas Tif2 binds both apo- and agonist-bound receptors (Musille et al., 2012). The discrete tissue expression of PGC1α and its inducible nature have made it an attractive therapeutic target; indeed, disruption of the LRH-1–PGC1α interaction has been proposed as a strategy to achieve tissue-specific inhibition of aromatase production in breast cancer (Safi et al., 2005). However, mechanisms through which PGC1α drives LRH-1 activation have not been delineated. Here, we present the first crystal structure of LRH-1 bound to PGC1α, allowing the visualization of the interface between these two partners. PGC1α bound LRH-1 with high affinity and induced strong communication within the LRH-1 AFS. Unlike Tif2, PGC1α did not induce conformational changes to AF-B or promote allosteric signaling from AF-B to the AFS, suggesting that the two coregulators use distinct mechanisms to activate LRH-1.

Materials and Methods

Materials and Reagents. Fluorescein (FAM)-labeled coregulator peptides were synthesized by RS Synthesis [silencing mediator of retinoic acid and thyroid hormone receptor (SMRT), Tif2, and SHP; Louisville, KY] or purchased from Thermo Fisher Scientific (PGC1α; Waltham, MA). Sequences of coregulators used in these assays are listed below. Unlabeled PGC1α peptide corresponding to NR box 2, used for crystallization and hydrogen-deuterium exchange (HDX), was purchased from RS Synthesis. Unlabeled Tif2 peptide corresponding to NR box 3, used for HDX, was purchased from RS Synthesis (all peptide sequences are listed later). Enantiomerically pure (1*S*,3a*S*)-5-hexyl-4-phenyl-3a-(1-phenylvinyl)-1,2,3,3a,6,6a-hexahydropentalen-1-ol (RR-RJW100) was synthesized as previously described (Stec, 2010; Whitby et al., 2011; Mays et al., 2016). For simplicity, this compound is referred to as "RJW100," a term previously used to describe a racemic mixture of RJW100 enantiomers (Whitby et al., 2011; Mays et al., 2016). The vector for His-tagged tobacco etch virus (TEV) protease was a gift from John Tesmer (University of Texas at Austin, Austin, TX). The pMSC7 vector was provided by John Sondek (University of North Carolina at Chapel Hill, Chapel Hill, NC).

Protein Purification. Purification of the LRH-1 LBD (residues 299–541) from the pMSC7 vector was carried out as in previous studies (Mays et al., 2016). In brief, protein expression was induced in *Escherichia coli* BL21 PLysS *E. coli* with 1 mM isopropyl 1-thio-β-galactopyranoside for 4 hours at 30°C. Following purification via nickel affinity chromatography, the protein was cleaved from the His tag using TEV protease. Cleaved protein was incubated with RJW100 overnight (10-fold molar excess) and then repurified by size-exclusion chromatography. The crystallization buffer consisted of 100 mM ammonium acetate (pH 7.4), 150 mM sodium chloride, 1 mM dithiothreitol, 1 mM EDTA, and 2 mM 3-[(3-cholamidopropyl)dimethylammonio]-1-propanesulfonic acid. For full-length (FL) LRH-1 purification, cell growth and fusion protein preparation were carried out as previously described (Weikum et al., 2016). To obtain pure human LRH-1–CYP7A1 promoter complex, double-stranded DNA was added to fusion protein at 1.2-fold molar excess. The complex was incubated with TEV protease overnight at 4°C for His-Small Ubiquitin-like Modifier tag cleavage. Samples were cleared of precipitate and loaded in a gel-filtration column for purification. Fractions containing the complex were pooled, concentrated, and frozen in liquid N_2. Aliquots were stored at −80°C for future use. Purity was assessed by SDS-PAGE and Coomassie staining and was found to be ~95% pure. Protein concentration was determined using the Pierce BCA Assay (Thermo Fisher Scientific).

Fluorescence Polarization Coregulator Binding Assays. FL LRH-1 (copurified with a portion of the CYP7A1 promoter) (Weikum et al., 2016) was incubated with RJW100 (10-fold molar excess) or an equal volume of dimethylsulfoxide overnight at 4°C. Binding of the ligand was verified using differential scanning fluorimetry, as previously described (Mays et al., 2016) (data not shown). The complex was serially diluted in assay buffer [20 mM HEPES (pH 7.4), 150 mM NaCl] in black-walled 384-well plates. Coregulator peptides, labeled at the N terminus with FAM, were then added to a final concentration of 50 nM. Fluorescence polarization was measured on a BioTek Neo plate reader (BioTek Instruments, Winooski, VT). Sequences of peptides used were as follows: Tif2 NR box 3, $^{+}H_3N$-PVSPKKKENALLRYLLDKDDT-CO_2^-; PGC1α NR box 2, $^{+}H_3N$-EEPSLLKKLLLAPA-CO_2^-; SHP NR box 1, $^{+}H_3N$-QGAASRPAILYALLSSSLK-CO_2^-; and SMRT, $^{+}H_3N$-TNMGLEAIIRKALMGKYDQW-CO_2^-). Assays were conducted three times in triplicate, using three separate preparations of protein. The exception was the *E. coli* phospholipid (PL)-SHP complex, which was assayed twice in triplicate. Data were combined and fitted to a single-site equilibrium binding equation with GraphPad Prism software (GraphPad Software, La Jolla, CA) to determine K_D. The significance of the difference in K_D values was determined using two-way analysis of variance followed by Sidak's multiple comparisons test. P values <0.05 were considered significant.

Crystallization. Protein ligand complexes were concentrated to 6.5 mg/ml and incubated with a peptide from PGC1α NR box 2 at 4-fold molar excess. Crystals were grown by hanging drop vapor diffusion at room temperature using 1 μl of protein and 1 μl of crystallant [0.05 M sodium acetate (pH 4.6), 14% polyethylene glycol 4000, and 15–21% glycerol] per drop.

Structure Determination. Crystals were flash frozen in liquid nitrogen using a cryoprotectant of crystallant with 30% glycerol. Data were collected remotely from the Argonne National Laboratory (South East Regional Collaborative Access Team, Lemont, IL) using the 22ID beamline. Data were processed using HKL2000 (HKL Research, Charlottesville, VA) (Otwinowski and Minor, 1997). The structure was phased by molecular replacement using Phaser in Phenix (Adams et al., 2010), with Protein Data Bank (PDB) 5L11 (ligand and coactivator removed) used as the search model. The model was refined using Phenix.refine (Adams et al., 2010), and figures were generated using PyMOL (v.1.3r1; Schrodinger, New York, NY).

HDX Mass Spectrometry. Purified LRH-1 LBD (His tag removed) was complexed with RJW100 by incubation overnight (10-fold molar excess) and then repurified by size exclusion into a buffer of 20 mM Tris-HCl (pH 7.5), 150 mM NaCl, and 5% glycerol. Additional RJW100 was added to the sized complex to ensure the receptor was saturated with ligand (5-fold molar excess). Solution-phase amide HDX experiments were carried out as described previously (Feng et al., 2016) using a fully automated system, in which sample handling was done using CTC HTS Twin PAL robots (LEAP Technologies, Carrboro, NC) housed inside a 4°C cabinet. In parallel reactions, 10 μM LRH-1 LBD-RJW100 complex was premixed with 4-fold molar excesses of peptides derived from either PGC1α ($^{+}H_3N$-EEPSLLKKLLLAPA-CO_2^-) or Tif2 ($^{+}NH_3$-KENALLRYLLDKDDT-CO_2^-). LRH-1–RJW100 with no coregulator added (designated "apo" for these studies) was used for comparison. The LRH-1–RJW100–coregulator complexes were allowed to form on ice and then subjected to HDX analysis. For the differential HDX experiments, 5-μl aliquots of 10 μM apo-LRH-1 or LRH-1–peptide complexes were mixed with 20 μl of D_2O-containing HDX buffer [20 mM Tris-HCl (pH 7.5), 150 mM NaCl, 5% glycerol] and incubated for a range of exchange times from 10 seconds to 1 hour before quenching the deuterium exchange with an acidic quench solution [5 M urea, 50 mM tris(2-carboxylethyl)phosphine, and 1% (v/v) trifluoroacetic acid, pH 2.4]. Protease digestion was performed in line with chromatography using an immobilized pepsin column. Mass spectra were acquired on a Q Exactive hybrid quadrupole-Orbitrap mass spectrometer (Thermo Fisher Scientific), and peptide identification from the tandem mass specrometry (MS/MS) data was done using the mascot database server (Matrix Science, London, UK). HDX experiments for each pairwise comparison (apo versus Tif2-bound LRH-1 LBD or apo versus PGC1α-bound LRH-1 LBD) were run separately under the same conditions, and percent deuterium exchange values for peptide isotopic envelopes at each time point were calculated and processed using HDX Workbench software developed in the Patrick Griffin Lab (The Scripps Research Institute, Jupiter, FL).

Model Construction for Molecular Dynamics Simulations. Six LRH-1 LBD complexes were prepared for molecular dynamics simulations, all containing the RJW100 ligand in the binding pocket. The first set was constructed from PDB 5L11 (with the Tif2 peptide bound). These included: 1) wild-type, 2) T352V, and 3) E534A protein. The second set was constructed from PBD 5UNJ (with the PGC1α peptide bound) and included: 4) wild-type, 5) T352V, and 6) E534A. All mutations were introduced in silico to the referenced structure coordinates. For consistency, all structures contained LRH-1 residues 300–540, and missing residues (i.e., that could not be modeled in the structures) were added to the models used in the simulations.

Molecular Dynamics Simulations. The complexes were solvated in an octahedral box of TIP3PB water with a 10-Å buffer around the protein complex. Na^+ and Cl^- ions were added to neutralize the protein and achieve physiologic conditions. All systems were using xleap, a component of AmberTools (version 15, ambermd.org). (Case et al., 2014) with the parm99-bsc0 forcefield (Pérez et al., 2007). Parameters for the RJW100 ligand were obtained using Antechamber (Wang et al., 2001) in AmberTools. All minimizations and simulations were performed with Amber14 (Case et al., 2014). Systems were minimized with 5000 steps of steepest decent followed by 5000 steps of conjugate gradient minimization with 500-kcal/mol•Å^2 restraints on all atoms. Restraints were removed from all atoms, excluding the atoms in both the ligand and the Tif2 and PGC1α peptides, and the previous minimization was repeated. The systems were heated from 0 to 300 K using a 100-ps run with constant volume periodic boundaries and 5-kcal/mol•Å^2 restraints on all protein and ligand atoms. Molecular dynamics (MD) equilibration was performed for 12 ns with 10-kcal/mol•Å^2 restraints on protein and ligand atoms using the constant-pressure, constant-temperature ensemble.

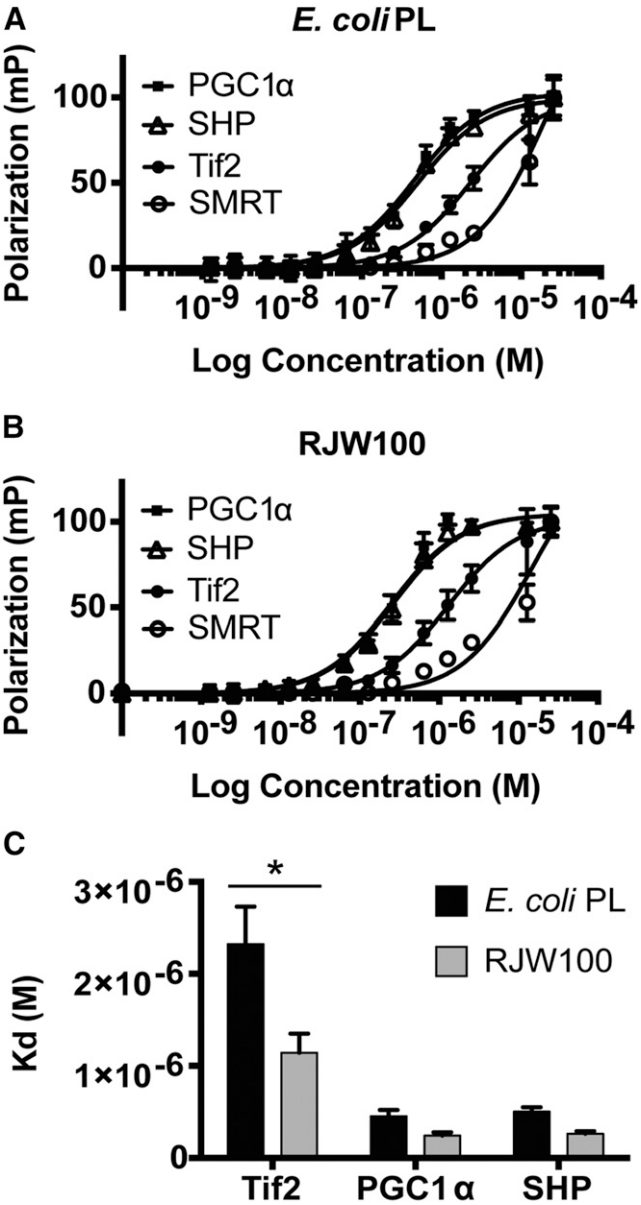

Fig. 1. Coregulator binding affinities for the LRH-1–RJW100 complex. Fluorescence polarization was used to determine binding affinities of LRH-1 for various coregulators. FL LRH-1 bound to PL from *E. coli* (A) or to RJW100 (B) was titrated in the presence of FAM-labeled coregulator peptides. (C) RJW100 increases the affinity of LRH-1 for Tif2. *$P < 0.05$.

TABLE 1
Affinities of LRH-1 for various coregulators
Values represent the mean ± S.E.M. of the K_D (μM) calculated from three separate experiments conducted in triplicate. Values in parentheses represent the goodness of fit (R^2).

	LBD		FL LRH-1	
	E. coli PL	RJW100	*E. coli* PL	RJW100
Tif2	8 ± 1 (0.99)	3.4 ± 0.3 (0.99)	2.3 ± 0.4 (0.93)	1.1 ± 0.2 (0.92)
PGC1α	0.8 ± 0.1 (0.98)	0.5 ± 0.1 (0.96)	0.45 ± 0.07 (0.95)	0.24 ± 0.04 (0.95)
SHP	0.9 ± 0.1 (0.99)	0.6 ± 0.1 (0.98)	0.50 ± 0.05 (0.99)	0.26 ± 0.03 (0.97)
SMRT	60 ± 30 (0.96)	25 ± 4 (0.99)	22 ± 9 (0.91)	20 ± 8 (0.91)

Restraints were reduced to 1 kcal/mol•Å^2 for an additional 10 ns of MD equilibration. Then, restraints were removed, and 500-ns production simulations were performed for each system in the constant-pressure, constant-temperature ensemble. A 2-fs time step was used, and all bonds between heavy atoms and hydrogens were fixed with the SHAKE algorithm (Ryckaert et al., 1977). A cutoff distance of 10 Å was used to evaluate long-range electrostatics with particle mesh Ewald and for van der Waals forces. Twenty-five thousand evenly spaced frames were taken from each simulation for analysis. Structural averaging and analysis were performed with the CPPTRAJ module (Roe and Cheatham, 2013) of AmberTools. The NetworkView plugin (Sethi et al., 2009) in VMD (Humphrey et al., 1996) and the Carma program (Glykos, 2006) were used to produce dynamic networks for each system. In brief, networks are constructed by defining all protein C-α atoms as nodes, using Cartesian covariance to measure communication within the network. Pairs of nodes that reside within a 4.5-Å cutoff for >75% of the simulation are connected via an edge. Edge weights are inversely proportional to the covariance between the nodes. Networks are resolved into communities, i.e., a group of nodes with correlated motions. Communities are generated using the Girvan-Newman algorithm. The minimum number of communities possible was generated while maintaining at least 98% maximum modularity (Newman, 2006). Suboptimal paths between the AF-B and AFS regions were identified using the Floyd-Warshall algorithm (Floyd, 1962). Suboptimal path analyses were performed using Carma and the subopt program in NetworkView. Cross-correlation matrices for C-α atoms in each system were computed with Carma.

Results

Coregulator Binding Affinities for Full-Length LRH-1. Previously published LRH-1 binding assays used isolated LBD due to difficulties purifying FL protein. We recently developed a method for FL LRH-1 purification and used this protein to investigate binding of FAM-conjugated coregulator peptides by fluorescence polarization. To stabilize the receptor and to provide a biologically relevant context, the protein was copurified with a portion of the CYP7A1 promoter containing the LRH-1 binding site (Weikum et al., 2016). The protein was purified from *E. coli* and contained a variety of bacterial phospholipids in the binding pocket (previously shown to act as weak activators) (Musille et al., 2012, 2016). We also determined affinities for various coregulators when FL LRH-1 was bound to the agonist RJW100. Binding curves from these experiments are shown in Fig. 1, and K_D values are summarized in Table 1. When *E. coli* PL occupied the binding pocket, PGC1α and SHP bound FL LRH-1 with higher affinity than Tif2 (~500 nM vs. 2.3 μM). The corepressor SMRT bound with much lower affinity (>20 μM). The addition of the LRH-1

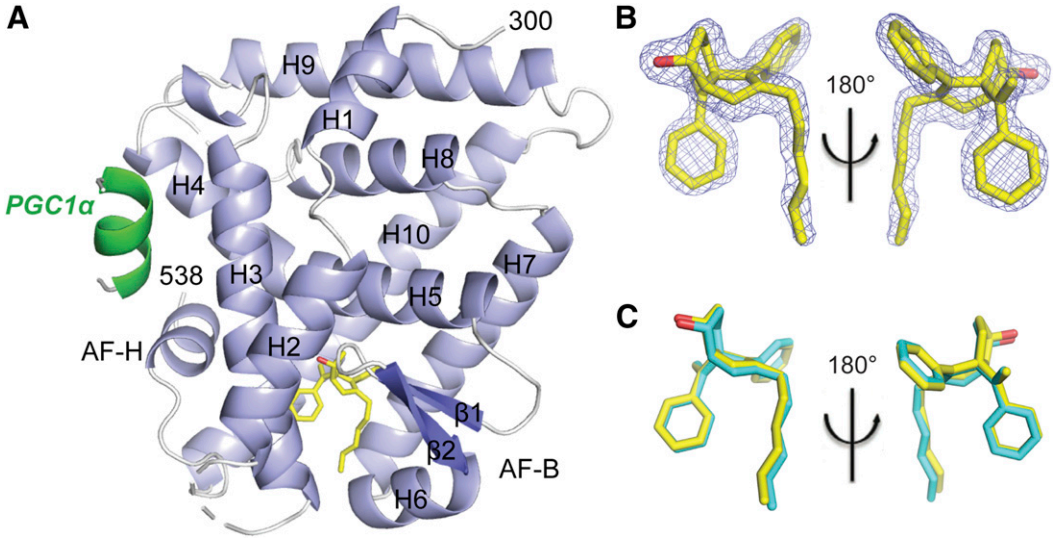

Fig. 2. Crystal structure of LRH-1–RJW100 with the PGC1α coactivator. (A) Overall structure, with α-helices shown in light blue, β-sheets in slate, and loops in white. The ligand is shown in yellow. PGC1α (green) is bound at the AFS. Dotted lines indicate regions that could not be modeled. (B) Electron density map surrounding the RJW100 ligand in the LRH-1–PGC1α complex (F_O-F_C omit map contoured to 3.0 σ). (C) Superposition of the ligand with PDB 5L11 (LRH-1–RJW100–Tif2) showing that it assumes a similar conformation in both structures. H, helix.

agonist RJW100 to the receptor increased affinity for Tif2 by around 2-fold ($P < 0.05$; Fig. 1C). Affinities for PGC1α and SHP trended higher in the presence of RJW100 (Table 1), but the differences were not statistically significant. As with native protein, PGC1α and SHP bound the LRH-1–RJW100 complex with higher affinity than Tif2 (1.1 ± 0.2 μM for Tif2 vs. 240 ± 40 nM for PGC1α; Table 1). To guide our crystallization efforts, and to provide some comparisons to previous studies, we also determined the affinities of the coregulators for purified LRH-1 LBD with or without RJW100. The K_D values were all higher than with FL protein, but they were proportionally the same (e.g., PGC1α bound with higher affinity than Tif2; Table 1). Together, these studies demonstrate the relatively high-affinity binding of PGC1α for LRH-1 and suggest that using isolated LBD for crystallography would provide an adequate model of this high-affinity interaction.

Crystal Structure of LRH-1 with PGC1α. To visualize the LRH-1–PGC1α interaction surface, we determined the crystal structure of the LRH-1 LBD, bound to a fragment of PGC1α, to a resolution of 1.95 Å (Fig. 2A; Table 2). The agonist RJW100, used to aid crystallization and to model the active state, is clearly bound in the pocket based on the surrounding electron density (Fig. 2B). The ligand adopts a similar position as in our previous structure (PDB 5L11) (Mays et al., 2016), where the LRH-1–RJW100 complex was crystallized with the Tif2 coactivator rather than PGC1α (Fig. 2C). Overall, LRH-1 conformation is not greatly changed when PGC1α, rather than Tif2, is bound (root mean square deviation = 0.5 Å). In the PGC1α structure, the loop connecting helix 2 to helix 3 is highly disordered and cannot be modeled (broken line in Fig. 2A); however, this region tends to be mobile when not stabilized by crystal contacts (such as the stabilization of this region that occurs in PDB 5L11). A second region of disorder occurs within the loop between helices 8 and 9, which prevented modeling of two residues (K462 and N463). This region also tends to be disordered when not stabilized by crystal contacts [for example, see PBD 4DOS (Musille et al., 2012)].

PGC1α is bound at the expected site at the AFS, a surface formed by portions of helices 3 and 4 and the activation function helix (AF-H) (Fig. 2). Although electron density is strong for the LXXLL consensus sequence and immediately adjacent amino acids, residues on either side of this sequence are disordered and cannot be modeled (i.e., residues 740–742 at the N terminus and 752–753 at the C terminus). Several PGC1α leucine side chains fit within the AFS and make hydrophobic interactions with the receptor (Fig. 3). We also examined the structure for a direct electrostatic interaction similar to the asparagine-lysine contact found to be important for the high-affinity interaction between peroxisome proliferator activated receptor λ and PGC1α (Li et al., 2008). LRH-1 has an aspartate residue (D372) that is in an analogous position to the peroxisome proliferator activated receptor λ asparagine; however, it is positioned 5.5 Å away from the nearest PGC1α lysine side chain and does not appear to be interacting (Fig. 3). On the other hand, LRH-1–Tif2 structures (both with *E. coli* PL and RJW100 bound) depict a direct contact with D372 via the side chain of residue R746 (seen in PDB 4PLE and 5L11, respectively; not shown) (Mays et al., 2016; Musille et al., 2016). Therefore, this contact does not appear to be correlated with the higher binding affinity of PGC1α for LRH-1 observed in our biochemical assay.

PGC1α Strengthens the Coactivator Charge Clamp and Communication within the LRH-1 AFS. An important driving force behind binding of coactivators and atypical corepressors to NRs is a charge clamp that neutralizes the helix dipole of the coregulator and secures it to the binding cleft in the AFS (Li et al., 2003). LRH-1 utilizes residues R361 and E534 to form the charge clamp, with an arginine substituted for the canonical lysine used by most NRs. We have shown that the presence of this charge clamp is closely associated with the strength of LRH-1 activation. For example, when LRH-1 is bound to weak PL activators, E534 is swung away from the Tif2 coactivator (>5 Å away), and the charge clamp is incomplete (Musille et al., 2016). However, when LRH-1 is bound to a specific and stronger PL agonist [dilauroylphosphatidylcholine (DLPC)], E534 makes direct

TABLE 2
X-ray data collection and refinement statistics
Values in parentheses indicate highest resolution shell.

Data Collection	LRH-1–RJW100–PGC1α
Space group	$P2_12_12$
Cell dimensions	
a, *b*, *c* (Å)	66.2, 84.0, 45.4
α, β, γ (°)	90, 90, 90
Resolution (Å)	50-1.95 (2.02-1.95)
R_{pim}	0.04 (0.18)
$I/\sigma I$	17.6 (2.1)
CC1/2 in highest shell	0.915
Completeness (%)	96.8 (83.8)
Redundancy	6.1 (5.0)
Refinement	
Resolution (Å)	1.95
No. reflections	18122
R_{work} / R_{free} (%)	19.9 / 22.7
No. atoms	
Protein	3847
Water	58
B-factors (Å^2)	
Protein	43.6
Ligand	35.2
Water	42.7
R.m.s. deviations	
Bond lengths (Å)	0.003
Bond angles (°)	0.489
Ramachandran favored (%)	97
Ramachandran outliers (%)	0
PDB accession code	5UNJ

R.m.s., root mean square.

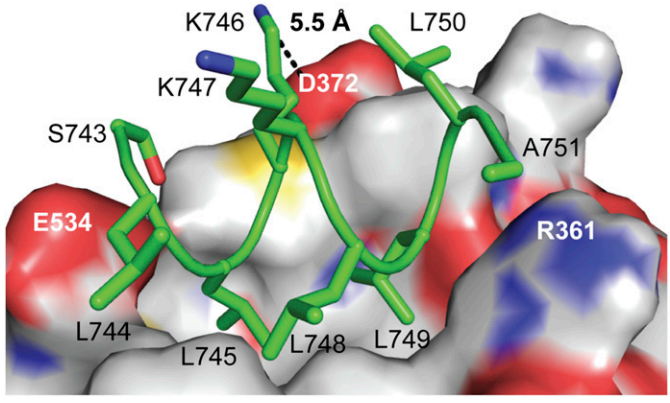

Fig. 3. Coregulator–LRH-1 binding interface. Molecular surface showing the interaction of PGC1α (green helix) with LRH-1. Surface is colored by atom type (carbon, gray; oxygen, red; nitrogen, blue; and sulfur yellow).

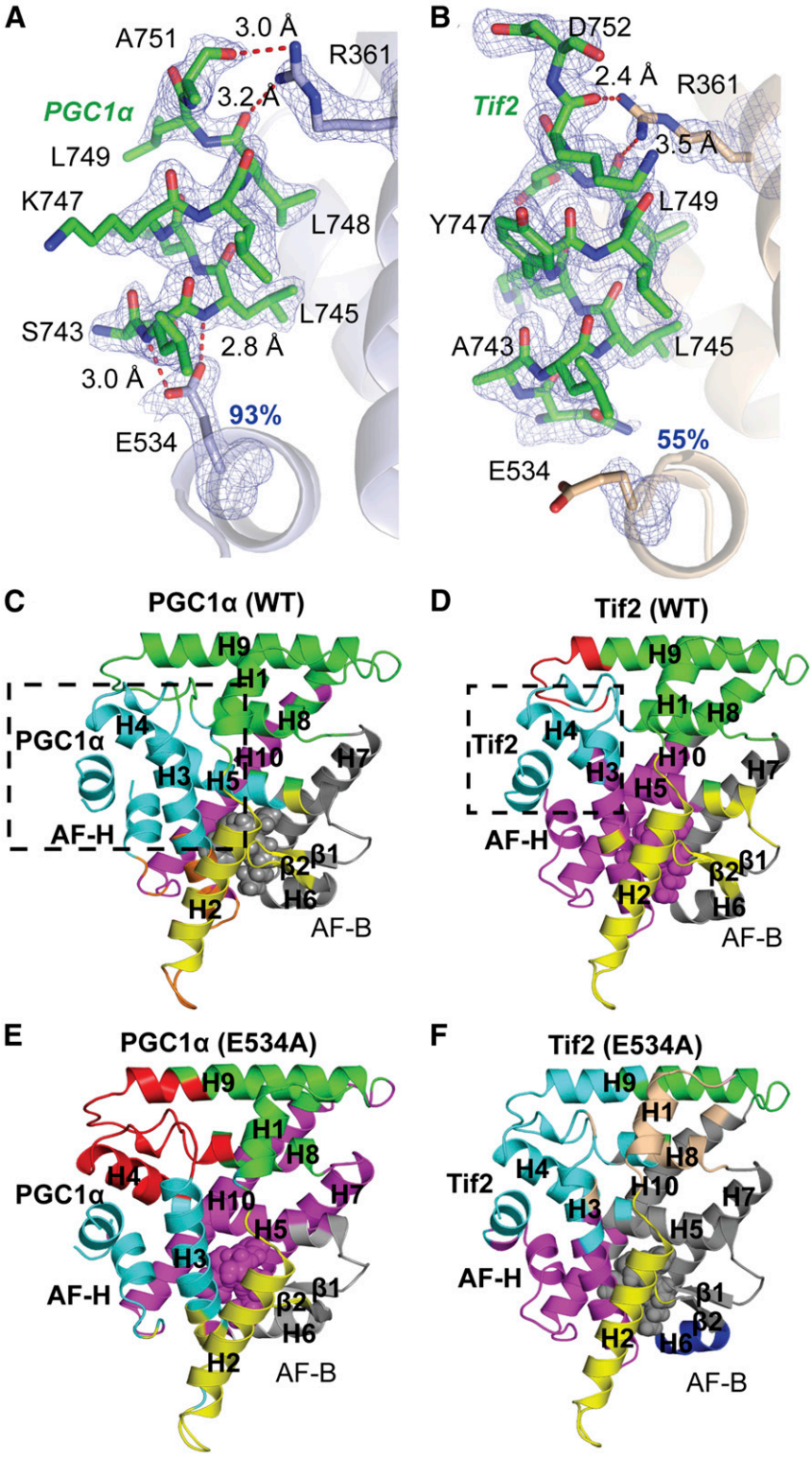

Fig. 4. A strong charge clamp occurs at the LRH-1–PGC1α interface. (A and B) Electron density maps showing strong evidence for placement of PGC1α (A) and Tif2 (from PDB 5L11) (B). Maps show F_O-F_C omit density contoured to 2.5 σ. Numbers in blue show the percentage of time that glutamate 534 interacted with each coregulator in 500-ns MDS. (C–F) Community analysis of MDS for either PGC1α with wild type (WT) LRH-1 (C), Tif2 with WT LRH-1 [from PBD 5L11(Mays et al., 2016)] (D), PGC1α with mutant (E534A) LRH-1 (E), or Tif2 with mutant (E534) LRH-1 (F). Dashed lines in (C) and (D) indicate the size and composition of the AFS community for WT LRH-1 in the presence of each coregulator. H, helix.

contact with Tif2 (Musille et al., 2016). In the LRH-1–PGC1α structure, the electron density provides strong evidence for the interaction with E534: the side chain engages backbone amide nitrogens of PGC1α residues L744 and L745 (Fig. 4A). Residue R361 has somewhat weaker electron density than E534 but clearly interacts with PGC1α residue A751 via NH1 and L749 via NH2 (Fig. 4A). In contrast, whereas the LRH-1–RJW100–Tif2 structure depicts similar interactions with R361, residue E534 has very weak electron density for the side chain (Fig. 4B). This weaker density is not related to resolution, since the Tif2 structure was determined at higher resolution than the PGC1α structure (1.85 vs. 1.95 Å). The disorder thus suggests that the E534 side chain is mobile when Tif2 is bound, and that the charge clamp is incomplete. Supporting this idea,

E534 maintains interactions with PGC1α for 93% of the time during 500-ns molecular dynamics simulations (MDS) versus only 55% of the time with Tif2. Interactions with R361 are maintained ~77% of the time for both coregulators in these simulations.

The stability of the E534-coregulator interaction is associated with correlated motion of residues within the LRH-1 AFS, indicative of strong communication in this region. This was determined using community analysis of the MDS (Fig. 4), which clusters residues into "communities" comprising residues that exhibit the greatest degree of correlated motion with one another. When PGC1α is bound, the coregulator and the entire LRH-1 AFS cluster as a single community that extends into helix 5 (Fig. 4C). However, the Tif2-bound AFS is split into two communities, the first comprising helix 4 and Tif2, and the second containing helix 3 and the AF-H (Fig. 4D). Mutation of residue E534 to alanine splits the AFS into two communities in the presence of PGC1α while not greatly affecting the AFS communities in the Tif2 structure (Fig. 4, E and F). These findings imply that PGC1α induces coordinated motion within the AFS, which is dependent, at least in part, on a stable interaction with LRH-1 residue E534.

Differential Effects of PGC1α and Tif2 on LRH-1 Allosteric Communication. In addition to the AFS, the helix 6/β-sheet region flanking the lower part of the binding pocket is important for LRH-1 activation and has been termed an alternative AFS (AF-B) (Musille et al., 2012). The PL LRH-1 agonist DLPC induces flexibility in AF-B (Musille et al., 2012) and promotes communication through the receptor from AF-B to the AFS (Musille et al., 2016). This communication is weaker when DLPC is bound in the presence of the corepressor SHP rather than Tif2, leading to the hypothesis that the AF-B transmits information about ligand status to the AFS to promote recruitment of appropriate coregulators (Musille et al., 2016). To understand how PGC1α affects this allosteric network, we used amide HDS mass spectrometry (HDX-MS) and MDS to compare changes in protein dynamics induced by PGC1α and Tif2. In both experiments, the agonist RJW100 was bound in the pocket to model the activated state. In the HDX-MS studies, less deuterium incorporation was

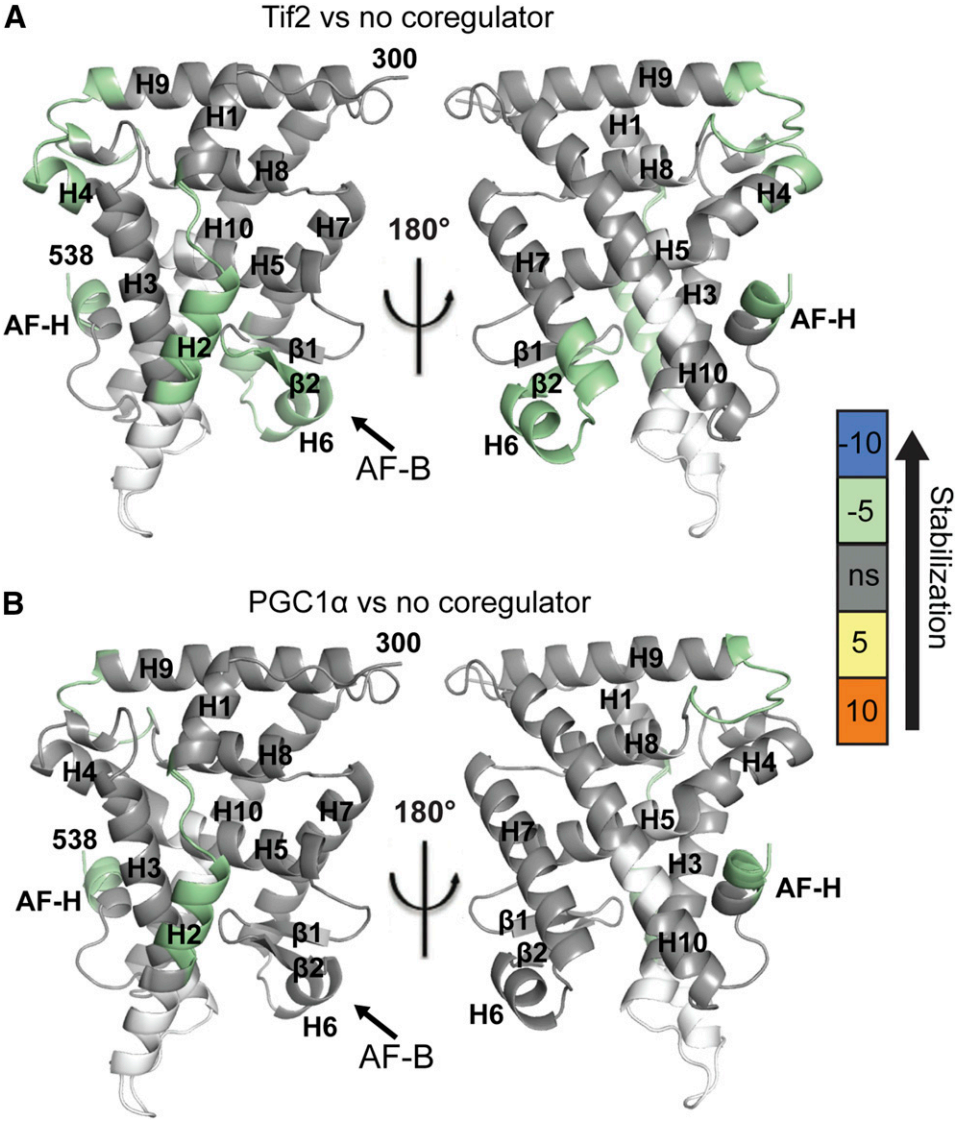

Fig. 5. Stabilization of the alternate AFS occurs upon Tif2 binding. Hydrogen deuterium exchange mass spectrometry was used to identify effects of Tif2 (A) and PGC1α (B) on LRH-1 dynamics. Each illustration is a map of differential deuterium incorporation of LRH-1 + coregulator versus LRH-1 only. The scale indicates the difference in percentage of deuterium incorporation: for example, negative numbers reflect a lower percentage of deuterium incorporation (less motion) for when the coregulator is bound versus no coregulator. A gray color indicates no significant difference in deuterium incorporation ("ns" in the scale bar). White indicates regions that were not detected by mass spectrometry. Results are mapped onto PDB 4DOS (Musille et al., 2012). H, helix.

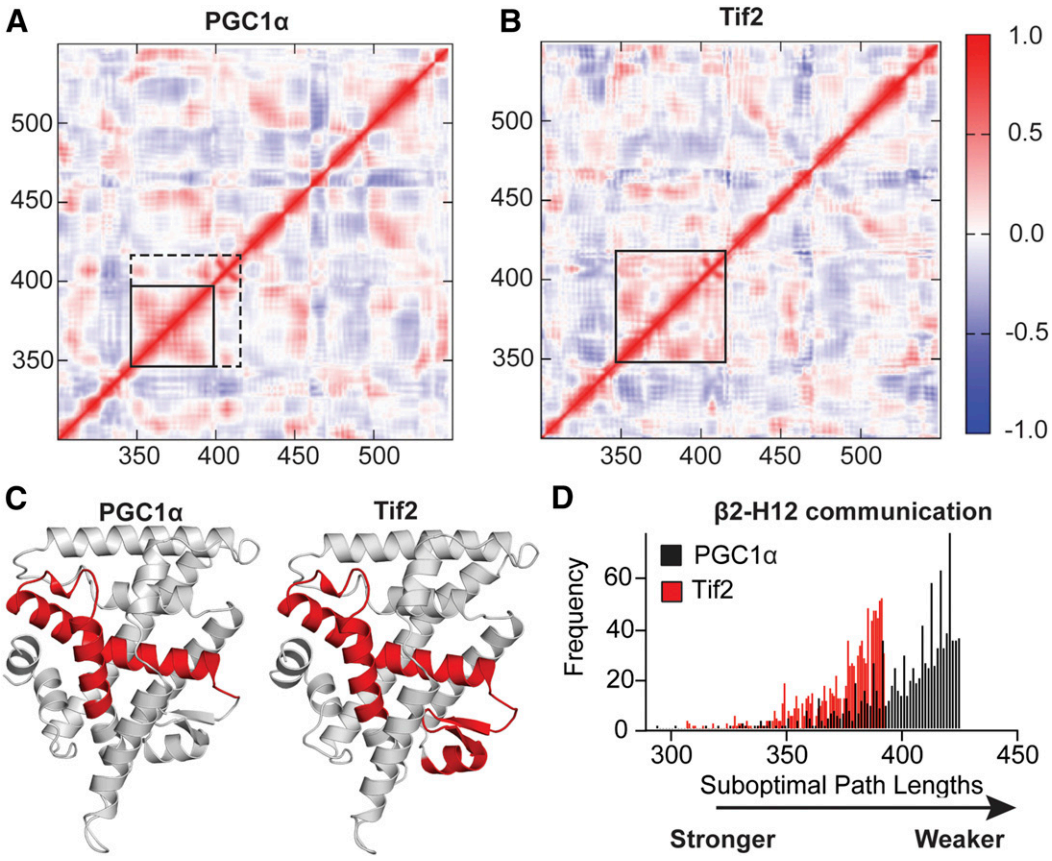

Fig. 6. Extended communication from AF-B to the canonical AFS with Tif2 but not PGC1α. (A and B) Covariance matrices for the MDS simulations with the LRH-1 bound to either PGC1α (A) or Tif2 (B). Solid squares surround the large region of correlated motion described in the text. The square with the dotted line shows the region of correlation in the Tif2 simulation that is not seen in the PGC1α simulation. (C) Shown in red are the regions identified in (A) and (B) mapped onto LRH-1 for each simulation. (D) The shortest 1000 suboptimal paths between LRH-1 β-sheet 2 in AF-B and the AFS for the PGC1α and Tif2 simulations, plotted as a histogram.

seen in the AF-H when either PGC1α or Tif2 was bound versus no coregulator (Fig. 5, A and B). This reduced motion at the site of coregulator binding was expected. However, the Tif2-bound receptor also exhibited reduced flexibility in AF-B, including helix 6, β2, and the bottom of helix 7, that was not seen for the LRH-1–PGC1α complex (Fig. 5, A and B).

Communication between AF-B and the AFS for each LRH-1–coregulator complex was determined by analysis of correlated motion between these regions in the MDS studies. Cross-correlation matrices were used to rank the degree of correlation between each pair of residues in the protein complexes on a scale of -1 to 1 [where -1 is perfect anticorrelation (opposite motion), 0 is no correlation, and 1 is perfect correlation] (Musille et al., 2016). Fig. 6, A and B depicts these values as a heat map, in which correlated motion is red and anticorrelated motion is blue. For the PGC1α complex, one of the largest regions of correlated motion is seen between residues 350 and 400 (Fig. 6A). Correlation in this vicinity is also seen for the Tif2 complex, but it is larger, extending to residue 420 (Fig. 6B). Mapping these regions onto LRH-1 shows that both coregulators induce correlated motion across helix 5 to helix 3, but Tif2 extends this correlation network into AF-B (Fig. 6C).

Strength of communication between AF-B and AF-H was further assessed by examination of the suboptimal paths between these sites. Communication between two distant regions of a receptor can occur through thousands of possible paths, and suboptimal-path analysis provides information about both the route and strength of allosteric communication. For this analysis, each Cα is defined as a "node," and the communication between each node is called an "edge." When considering communication between two distant nodes, a communication path can be drawn as a chain of edges connecting them. Edges are weighted by their correlated motion in the MD trajectory, such that correlation is inversely proportional to edge weight (Musille et al., 2016). Therefore, the sum of edges along a path between two distant nodes becomes lower as strength of communication increases. The path for which the sum of the edges is lowest is called the shortest, or optimal, path. The optimal path and a set of suboptimal paths with the shortest lengths are thought to convey the greatest amount of communication between two distant nodes (Sethi et al., 2009; Musille et al., 2016). For our analysis, we considered the shortest 1000 suboptimal paths between β2 and the AF-H for each LRH-1–coregulator complex. The routes taken by the paths were not substantially different in the presence of either coregulator: they traversed helix 5 and went through helix 3 to the AF-H (not shown). However, the strength of the communication was significantly weaker when PGC1α was bound compared with Tif2. This is seen in the plot of suboptimal-path lengths, which shows shorter lengths when Tif2 is bound (Fig. 6D). Together with the HDX-MS results, these findings indicate that Tif2 affects

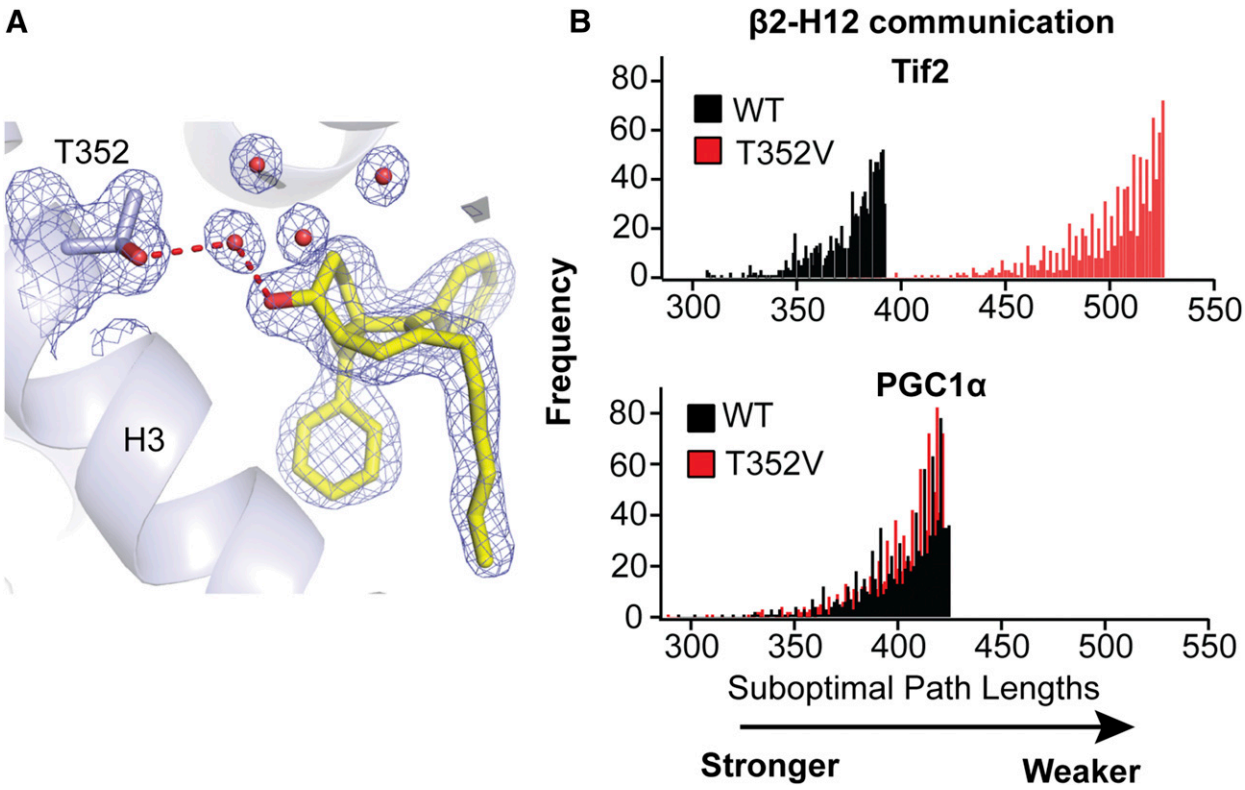

Fig. 7. Contribution of the ligand to allosteric signaling between two LRH-1 activation surfaces. (A) Electron density map ($2F_O$-F_C, contoured to 1 σ) showing evidence for the water-mediated interaction of the RJW100 ligand with LRH-1. (B) Histogram showing the distribution of 1000 shortest suboptimal paths for wild-type (WT) or T352V LRH-1 when bound to either PGC1α (top panel) or Tif2 (bottom panel). H, helix.

LRH-1 conformation at AF-B and promotes communication between AF-B and the AFS, whereas PGC1α acts primarily at the AFS.

Ligand Participation in Allosteric Signaling within the LRH-1–Tif2 Complex. We previously identified a water-mediated interaction with residue T352 as being important for LRH-1 activation by the RJW100 agonist (Mays et al., 2016). In the LRH-1–PGC1α structure, the ligand is oriented very similarly as in the LRH-1–Tif2 complex (Fig. 2), and it makes contact with the T352-coordinated water via the hydroxyl group (Fig. 7A). However, this interaction is predicted to be much less stable in the presence of PGC1α versus Tif2 (occurring 33 and 68% of the time, respectively, over the course of 500-ns MDS). Introduction of threonine to valine mutation at position 352 in the MDS had very little effect on suboptimal-path length between AF-B and the AFS for the LRH-1–PGC1α complex (Fig. 7B). In contrast, a dramatic lengthening of the suboptimal paths occurred for the T352V mutant in the LRH-1—Tif2 complex (Fig. 7B). This is consistent with our observations that AF-B to AFS communication is more important for Tif2 than PGC1α and further indicates that the ligand plays an active role in this communication via the T352 interaction.

Discussion

Regulation of NR activity is complex, involving a dynamic interplay of ligand binding, post-translational modifications, and coregulator associations. Study of LRH-1 regulation is particularly challenging, since the endogenous ligand for this receptor is unknown, and since only a few coregulators have been crystallized with LRH-1 previously [i.e., Tif2 (Musille et al., 2012, 2016; Mays et al., 2016), SHP (Li et al., 2005; Ortlund et al., 2005), and DAX (dosage-sensitive sex reversal, adrenal hypoplasia critical region, on chromosome X, gene 1, Sablin et al., 2008)]. Tif2 is the only coactivator among these, which greatly limited the ability to investigate LRH-1–coactivator interactions. The LRH-1–PGC1α structure thus makes a significant contribution to our understanding of its regulation by coactivators. Notably, PGC1α interacts stably with LRH-1 residue E534. This interaction is clearly seen in the electron density maps, confirmed by MDS, and required for the large region of coordinated motion within the LRH-1 AFS and with the PGC1α peptide (Fig. 4). In contrast, Tif2 did not interact with E534 in the RJW100–LRH-1 crystal structure and engaged this residue approximately half of the time compared with PGC1α during MDS. Unfortunately, only a short stretch of the PGC1α peptide could be modeled in our structure, which may have prevented the identification of other important interactions. In particular, a PGC1α proline residue was hypothesized to be important for LRH-1 binding, as is the case for the LRH-1–SHP complex (Ortlund et al., 2005). However, we were not able to model this proline residue due to weak electron density. A natural extension of this work would be to investigate the interaction surface of LRH-1 with a larger portion of PGC1α. Although the degree of intrinsic disorder of PGC1α would likely make crystallization of the complex difficult, HDX-MS experiments with estrogen related receptor γ and a large-domain PGC1α have been successful in the past (Devarakonda et al., 2011). This approach could be a

useful way to study the effect of PGC1α on LRH-1 conformation (and vice versa), as well as the role particular residues play at the interface of the two partners.

In addition to the differential effects at the AFS, PGC1α and Tif2 had strikingly different effects on LRH-1 dynamics at AF-B, seen in both solution-based and in silico experiments. HDX-MS showed no significant effect on AF-B when PGC1α was bound, whereas Tif2 caused reduced flexibility at this site. Moreover, MDS showed a greater strength of intramolecular communication from AF-B to AF-H in the presence of Tif2 (Fig. 6). Collectively, we identified two distinct mechanisms through which coregulators alter LRH-1 conformation in the presence of the same LRH-1 agonist. The reason for the differing mechanisms of activation is unclear, but a possible explanation lies in the fact that Tif2 is expressed at a fairly constant level, whereas PGC1α is highly inducible. Tif2 has a relatively low binding affinity for LRH-1 (Fig.: 1), and it is plausible that recruitment of Tif2 is driven mainly by availability of an activating ligand. On the other hand, PGC1α-driven activation likely originates from upstream signaling pathways, causing, for example, cAMP generation and consequent PGC1α production. Strong action of PGC1α at the LRH-1 AFS could then promote a receptor conformational change that favors agonist binding and transcriptional activation. This could thus serve as a platform through which LRH-1 could drive alternative transcriptional programs in response to specific stressors. Although additional work is needed to support this hypothesis, the idea that Tif2-mediated activation is more reliant on signaling from the ligand is supported by the fact that communication from AF-B to the AFS is greatly weakened upon mutation of an RJW100 contact that is critical for activation of LRH-1 by this ligand (Mays et al., 2016) (Fig. 7). Strong communication between AF-B and the ligand is a hallmark of activating ligands, as shown in our previous publications (Musille et al., 2012, 2016; Mays et al., 2016). The identification of separate mechanisms of action of two major LRH-1 coactivators has potential to be exploited for selective targeting of desired LRH-1 signaling pathways as a novel therapeutic strategy for the treatment of metabolic diseases and cancer.

Acknowledgments

The authors thank Sally Bloodworth (University of Southampton, UK) for assistance with synthetic chemistry.

Authorship Contributions

Participated in research design: Mays, Okafor, Dharmarajan, Griffin, Ortlund.

Conducted experiments: Mays, Okafor, Tuntland, Dharmarajan.

Contributed new reagents or analytic tools: Stec, Whitby.

Performed data analysis: Mays, Okafor, Dharmarajan, Griffin, Ortlund.

Wrote or contributed to the writing of the manuscript: Mays, Okafor, Tuntland, Whitby, Dharmarajan, Stec, Griffin, Ortlund.

References

Adams PD, Afonine PV, Bunkóczi G, Chen VB, Davis IW, Echols N, Headd JJ, Hung LW, Kapral GJ, Grosse-Kunstleve RW, et al. (2010) PHENIX: a comprehensive Python-based system for macromolecular structure solution. *Acta Crystallogr D Biol Crystallogr* **66**:213–221.

Bayrer JR, Mukkamala S, Sablin EP, Webb P, and Fletterick RJ (2015) Silencing LRH-1 in colon cancer cell lines impairs proliferation and alters gene expression programs. *Proc Natl Acad Sci USA* **112**:2467–2472.

Bianco S, Brunelle M, Jangal M, Magnani L, and Gévry N (2014) LRH-1 governs vital transcriptional programs in endocrine-sensitive and -resistant breast cancer cells. *Cancer Res* **74**:2015–2025.

Bolado-Carrancio A, Riancho JA, Sainz J, and Rodríguez-Rey JC (2014) Activation of nuclear receptor NR5A2 increases Glut4 expression and glucose metabolism in muscle cells. *Biochem Biophys Res Commun* **446**:614–619.

Case D, Babin V, Berryman J, Betz R, Cai Q, Cerutti D, Cheatham Iii T, Darden T, Duke R and Gohlke H (2014) Amber 14.

Chand AL, Herridge KA, Thompson EW, and Clyne CD (2010) The orphan nuclear receptor LRH-1 promotes breast cancer motility and invasion. *Endocr Relat Cancer* **17**:965–975.

Devarakonda S, Gupta K, Chalmers MJ, Hunt JF, Griffin PR, Van Duyne GD, and Spiegelman BM (2011) Disorder-to-order transition underlies the structural basis for the assembly of a transcriptionally active PGC-1α/ERRγ complex. *Proc Natl Acad Sci USA* **108**:18678–18683.

Feng L, Dharmarajan V, Serrao E, Hoyte A, Larue RC, Slaughter A, Sharma A, Plumb MR, Kessl JJ, Fuchs JR, et al. (2016) The Competitive Interplay between Allosteric HIV-1 Integrase Inhibitor BI/D and LEDGF/p75 during the Early Stage of HIV-1 Replication Adversely Affects Inhibitor Potency. *ACS Chem Biol* **11**: 1313–1321.

Finck BN and Kelly DP (2006) PGC-1 coactivators: inducible regulators of energy metabolism in health and disease. *J Clin Invest* **116**:615–622.

Floyd RW (1962) Algorithm 97: shortest path. *Commun ACM* **5**:345.

Glykos NM (2006) Software news and updates. Carma: a molecular dynamics analysis program. *J Comput Chem* **27**:1765–1768.

Humphrey W, Dalke A, and Schulten K (1996) VMD: visual molecular dynamics. *J Mol Graph* **14**:33–38, 27–28.

Lee JM, Lee YK, Mamrosh JL, Busby SA, Griffin PR, Pathak MC, Ortlund EA, and Moore DD (2011) A nuclear-receptor-dependent phosphatidylcholine pathway with antidiabetic effects. *Nature* **474**:506–510.

Li Y, Choi M, Suino K, Kovach A, Daugherty J, Kliewer SA, and Xu HE (2005) Structural and biochemical basis for selective repression of the orphan nuclear receptor liver receptor homolog 1 by small heterodimer partner. *Proc Natl Acad Sci USA* **102**:9505–9510.

Li Y, Kovach A, Suino-Powell K, Martynowski D, and Xu HE (2008) Structural and biochemical basis for the binding selectivity of peroxisome proliferator-activated receptor gamma to PGC-1alpha. *J Biol Chem* **283**:19132–19139.

Li Y, Lambert MH, and Xu HE (2003) Activation of nuclear receptors: a perspective from structural genomics. *Structure* **11**:741–746.

Lin J, Handschin C, and Spiegelman BM (2005) Metabolic control through the PGC-1 family of transcription coactivators. *Cell Metab* **1**:361–370.

Lin Q, Aihara A, Chung W, Li Y, Huang Z, Chen X, Weng S, Carlson RI, Wands JR, and Dong X (2014) LRH1 as a driving factor in pancreatic cancer growth. *Cancer Lett* **345**:85–90.

Lu TT, Makishima M, Repa JJ, Schoonjans K, Kerr TA, Auwerx J, and Mangelsdorf DJ (2000) Molecular basis for feedback regulation of bile acid synthesis by nuclear receptors. *Mol Cell* **6**:507–515.

Mamrosh JL, Lee JM, Wagner M, Stambrook PJ, Whitby RJ, Sifers RN, Wu SP, Tsai MJ, Demayo FJ, and Moore DD (2014) Nuclear receptor LRH-1/NR5A2 is required and targetable for liver endoplasmic reticulum stress resolution. *eLife* **3**:e01694.

Mays SG, Okafor CD, Whitby RJ, Goswami D, Stec J, Flynn AR, Dugan MC, Jui NT, Griffin PR, and Ortlund EA (2016) Crystal Structures of the Nuclear Receptor, Liver Receptor Homolog 1, Bound to Synthetic Agonists. *J Biol Chem* **291**: 25281–25291.

Musille PM, Kossmann BR, Kohn JA, Ivanov I, and Ortlund EA (2016) Unexpected Allosteric Network Contributes to LRH-1 Co-regulator Selectivity. *J Biol Chem* **291**:1411–1426.

Musille PM, Pathak MC, Lauer JL, Hudson WH, Griffin PR, and Ortlund EA (2012) Antidiabetic phospholipid-nuclear receptor complex reveals the mechanism for phospholipid-driven gene regulation. *Nat Struct Mol Biol* **19**:532–537.

Nadolny C and Dong X (2015) Liver receptor homolog-1 (LRH-1): a potential therapeutic target for cancer. *Cancer Biol Ther* **16**:997–1004.

Newman ME (2006) Modularity and community structure in networks. *Proc Natl Acad Sci USA* **103**:8577–8582.

Oosterveer MH, Mataki C, Yamamoto H, Harach T, Moullan N, van Dijk TH, Ayuso E, Bosch F, Postic C, Groen AK, et al. (2012) LRH-1-dependent glucose sensing determines intermediary metabolism in liver. *J Clin Invest* **122**: 2817–2826.

Ortlund EA, Lee Y, Solomon IH, Hager JM, Safi R, Choi Y, Guan Z, Tripathy A, Raetz CR, McDonnell DP, et al. (2005) Modulation of human nuclear receptor LRH-1 activity by phospholipids and SHP. *Nat Struct Mol Biol* **12**:357–363.

Otwinowski Z and Minor W (1997) Processing of x-ray diffraction data collected in oscillation mode. *Methods Enzymol* **276**:307–326.

Pascal BD, Willis S, Lauer JL, Landgraf RR, West GM, Marciano D, Novick S, Goswami D, Chalmers MJ, and Griffin PR (2012) HDX workbench: software for the analysis of H/D exchange MS data. *J Am Soc Mass Spectrom* **23**: 1512–1521.

Pérez A, Marchán I, Svozil D, Sponer J, Cheatham, 3rdTE, Laughton CA, and Orozco M (2007) Refinement of the AMBER force field for nucleic acids: improving the description of α/γ conformers. *Biophys J* **92**:3817–3829.

Roe DR and Cheatham, 3rdTE (2013) PTRAJ and CPPTRAJ: software for processing and analysis of molecular dynamics trajectory data. *J Chem Theory Comput* **9**: 3084–3095.

Ryckaert J-P, Ciccotti G, and Berendsen HJ (1977) Numerical integration of the cartesian equations of motion of a system with constraints: molecular dynamics of n-alkanes. *J Comput Phys* **23**:327–341.

Sablin EP, Woods A, Krylova IN, Hwang P, Ingraham HA, and Fletterick RJ (2008) The structure of corepressor Dax-1 bound to its target nuclear receptor LRH-1. *Proc Natl Acad Sci USA* **105**:18390–18395.

Safi R, Kovacic A, Gaillard S, Murata Y, Simpson ER, McDonnell DP, and Clyne CD (2005) Coactivation of liver receptor homologue-1 by peroxisome proliferator-activated receptor gamma coactivator-1alpha on aromatase promoter II and its inhibition by activated retinoid X receptor suggest a novel target for breast-specific antiestrogen therapy. *Cancer Res* **65**: 11762–11770.

Schoonjans K, Annicotte J-S, Huby T, Botrugno OA, Fayard E, Ueda Y, Chapman J, and Auwerx J (2002) Liver receptor homolog 1 controls the expression of the scavenger receptor class B type I. *EMBO Rep* **3**:1181–1187.

Sethi A, Eargle J, Black AA, and Luthey-Schulten Z (2009a) Dynamical networks in tRNA:protein complexes. *Proc Natl Acad Sci USA* **106**:6620–6625.

Shin DJ and Osborne TF (2008) Peroxisome proliferator-activated receptor-gamma coactivator-1alpha activation of CYP7A1 during food restriction and diabetes is still inhibited by small heterodimer partner. *J Biol Chem* **283**: 15089–15096.

Stec J(2010) Tandem Reaction Sequences on a Zirconocene Template, in *Chemistry*, Ph.D. Thesis, University of Southampton, Southampton, UK.

Stein S, Oosterveer MH, Mataki C, Xu P, Lemos V, Havinga R, Dittner C, Ryu D, Menzies KJ, Wang X, et al. (2014) SUMOylation-dependent LRH-1/PROX1 interaction promotes atherosclerosis by decreasing hepatic reverse cholesterol transport. *Cell Metab* **20**:603–613.

Thiruchelvam PT, Lai CF, Hua H, Thomas RS, Hurtado A, Hudson W, Bayly AR, Kyle FJ, Periyasamy M, Photiou A, et al. (2011) The liver receptor homolog-1 regulates estrogen receptor expression in breast cancer cells. *Breast Cancer Res Treat* **127**:385–396.

Wagner M, Choi S, Panzitt K, Mamrosh JL, Lee JM, Zaufel A, Xiao R, Wooton-Kee R, Ståhlman M, Newgard CB, et al. (2016) Liver receptor homolog-1 is a critical determinant of methyl-pool metabolism. *Hepatology* **63**:95–106.

Wang J, Wang W, Kollman PA, and Case DA (2001) Antechamber: an accessory software package for molecular mechanical calculations. *J Am Chem Soc* **222**:U403.

Weikum ER, Tuntland ML, Murphy MN, and Ortlund EA (2016) A Structural Investigation into Oct4 Regulation by Orphan Nuclear Receptors, Germ Cell Nuclear Factor (GCNF), and Liver Receptor Homolog-1 (LRH-1). *J Mol Biol* **428** (24 Pt B): 4981–4992.

Whitby RJ, Stec J, Blind RD, Dixon S, Leesnitzer LM, Orband-Miller LA, Williams SP, Willson TM, Xu R, Zuercher WJ, et al. (2011) Small molecule agonists of the orphan nuclear receptors steroidogenic factor-1 (SF-1, NR5A1) and liver receptor homologue-1 (LRH-1, NR5A2). *J Med Chem* **54**:2266–2281.

Xu P, Oosterveer MH, Stein S, Demagny H, Ryu D, Moullan N, Wang X, Can E, Zamboni N, Comment A, et al. (2016) LRH-1-dependent programming of mitochondrial glutamine processing drives liver cancer. *Genes Dev* **30**:1255–1260.

Address correspondence to: Eric A. Ortlund, 1510 Clifton Road NE, Rollins Research Center G235, Atlanta, GA 30322. E-mail: eortlun@emory.edu